Recombination dynamics in wurtzite InP nanowires

S. Crankshaw,[1] S. Reitzenstein,[3] L. C. Chuang,[2] M. Moewe,[2] S. Münch,[3] C. Böckler,[3] A. Forchel,[3] and C. Chang-Hasnain[1,2]
[1]*Applied Science and Technology, University of California at Berkeley, Berkeley, California 94720, USA*
[2]*Department of Electrical Engineering and Computer Sciences, University of California at Berkeley, Berkeley, California 94720, USA*
[3]*Technische Physik, Physikalisches Institut, Universität Würzburg, Am Hubland, D-97074 Würzburg, Germany*
(Received 28 November 2007; revised manuscript received 3 March 2008; published 5 June 2008)

We report time-resolved photoluminescence investigations of as-grown wurtzite InP nanowires ($d_{av}=16$ nm) on a (111) silicon substrate as a function of emission energy, temperature, and excitation fluence. The observed luminescence transients are well described by a biexponential decay process, with $\tau_{fast}\sim 0.3-0.7$ ns and $\tau_{slow}\sim 2-5$ ns, which does not originate from band bending induced by surface states. The trends associated with the decay characteristics instead point to size-dependent localization effects in the narrow nanowires.

DOI: 10.1103/PhysRevB.77.235409 PACS number(s): 78.47.Cd, 78.55.Cr, 78.67.−n

I. INTRODUCTION

Semiconductor nanowires (NWs) have attracted great interest in recent years both for basic studies of one-dimensional physics and as building blocks for nanoscale devices. Literature now exists for many III-V and II-VI material systems and with various growth modes, such as laser-assisted catalytic growth[1] and chemical beam epitaxy,[2] as well as some noncatalytic methods[3] such as selective-area epitaxy.[4,5] The vapor-liquid-solid (VLS) growth mechanism[6] has been a popular mode of synthesis,[7–10] in which gas-phase reactants saturate a liquid metal catalyst and precipitate underneath to form a crystalline solid. When grown on [111]-oriented substrates, nanowires tend to vertically align, such that they are unclad, freestanding structures with a lateral dimension primarily determined by the size of the catalyst metal droplet.

Much work has been dedicated to exploring the growth window[8,11,12] and optimizing the multitude of parameters involved in any synthesis method, including the VLS growth of InP nanowires that are the subject of this study. One striking feature of InP nanowires, as well as other typically zinc blende III-V materials, is their ability to crystallize in the wurtzite structure. Although bulk InP always occurs in a zinc blende crystal structure, both zinc blende[3,7,13] and wurtzite[2,4,14] crystal phases have been reported for InP nanowires, indeed sometimes simultaneously.[11] Various theoretical[15,16] and experimental[4,11,14] reports indicate a substantial blueshift of the emission energy of wurtzite InP compared to zinc blende InP, although the range of reported values also significantly varies. These have involved wires with diameters larger than twice the exciton Bohr radius (~9 nm) in bulk InP, such that quantum confinement is not a contributing factor.

In this paper, we report a systematic study of the recombination dynamics of wurtzite InP NWs with an average diameter of 16 nm as a function of emission energy, temperature, and excitation fluence. In III-V systems, time-resolved photoluminescence (PL) has been used in the past to study one-dimensional structures such as V-groove[17–20] and etched[21] quantum wires as well as self-assembled quantum dash structures,[22] but few reports have mentioned the carrier dynamics in freestanding nanowires.[3,23] Other groups have performed time-resolved measurements on II-VI nanowires such as ZnO,[24] ZnSe,[25] and CdS,[26] revealing complex recombination dynamics in these structures. The information about carrier lifetimes extracted from such measurements is extremely relevant for designing optoelectronic devices, as well as of basic scientific interest, especially given the wurtzite crystal structure of the InP nanowires. Furthermore, because the NWs are directly grown on (111) silicon, we can directly perform photoluminescence characterization on the as-grown samples without having to remove them from the substrate. We therefore establish baseline characteristics of the as-grown sample to ascertain how subsequent surface treatment or fabrication steps alter the optical properties of the nanowires, which one can expect to sensitively depend on the surface modifications given the large surface-to-volume ratio.

II. EXPERIMENTAL DETAILS

The InP nanowires used in this study are grown via the VLS method in a metal-organic chemical vapor deposition reactor. A solution of gold nanoparticles nominally 10 nm in diameter is deposited onto a deoxidized (111) silicon wafer and annealed at 640 °C in the reaction chamber for 3 min under a flow of H_2. The wafer platter is subsequently ramped down to the growth temperature of 470 °C, and the metal-organic reactants, TMIn (trimethylindium) and TBP (tertiarybutylphosphene) , are introduced with a V/III ratio of 61 as determined from the mass-flow controllers at the input. After 3 min of growth, the temperature is decreased to ambient in an H_2 environment. Further details about the growth are described elsewhere.[9]

A scanning electron micrograph of a typical high-density sample area is shown in Fig. 1, from which the vertical, epitaxial growth from the substrate is evident. This picture shows a region on the substrate with a density of ~150 nanowires/μm^2, although the coverage is inhomogeneous and areas with low nanowire densities are also found. The wires are typically ≤ 1 μm in length, with an average diameter of 16 nm ($\sigma=3.4$ nm), which includes an ~2 nm thick amorphous layer surrounding the nanowire itself. Transmis-

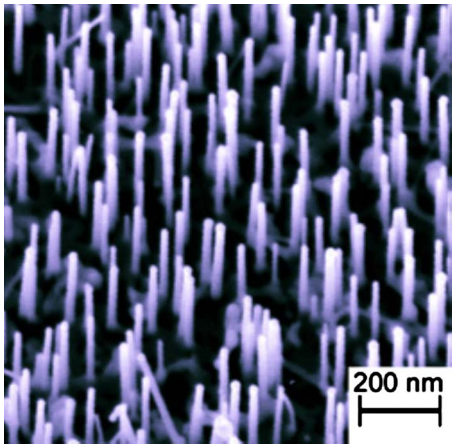

FIG. 1. (Color online) 20°-tilted scanning electron microscopy picture of the as-grown InP nanowires on a (111) Si substrate. The μ-PL measurements are performed without removing the wires from the substrate.

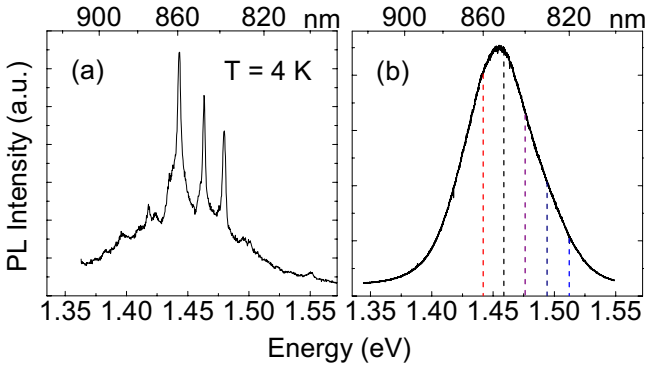

FIG. 2. (Color online) T=4 K. (a) Representative μ-PL spectrum under low excitation conditions, showing narrow luminescence lines from individual nanowires. (b) Inhomogeneously broadened PL spectrum under high excitation conditions, representing the ensemble of nanowires. Vertical lines indicate the detection energies where transient measurements were performed.

sion electron microscope investigations have further revealed that the nanowires crystallize in a wurtzite phase, which exhibit extremely smooth sidewalls with no evidence of rotational twins along the entire length. High-resolution transmission electron microscopy (TEM) images also show an AB rather than ABC stacking pattern, further confirming the wurtzite structure.

Microphotoluminescence (μ-PL) measurements are performed for optical characterization of the InP nanowires. The as-grown samples are mounted in a continuous-flow helium cryostat, and an excitation beam from an argon-pumped Ti-:sapphire laser is focused onto the sample through a numerical aperture=0.4 microscope objective with a spot size of ~3 μm at low intensities. The laser provides ~150 fs pulses at 1.67 eV to the sample, with a repetition rate of 82 MHz. The sample luminescence is collected by the same microscope objective and passes through a 0.55 m spectrometer to a nitrogen-cooled silicon charge-coupled device for time-integrated photoluminescence measurements. Time-resolved measurements are achieved by the time-correlated photon-counting method, where the detector is instead a photomultiplier tube in conjunction with single-photon-counting electronics, providing a timing resolution of ~100 ps. The spectral window for the time-resolved measurements is 5 meV.

The PL characterization is performed on the as-grown nanowire sample, without the wires being dispensed onto a separate substrate before measurement. Still, contributions from individual wires are discernable in the time-integrated μ-PL measurements at very low excitation intensities (<10 W/cm^2). These measurements extremely reveal narrow emission linewidths, typically 2–6 meV at low temperatures, as shown in Fig. 2(a). This is much narrower than that reported by other groups, in the range of 20–100 meV.[3,4,7,13] Multiple factors may contribute to this comparatively small linewidth. One is that the nanowires here are free of rotational twins and polytyping that some groups have seen in TEM investigations of InP nanowires.[8] However, ~20 meV linewidths have also been reported in PL measurements on pure wurtzite InP nanowires.[4] We believe that a primary reason for the narrow linewidths may be the pristine surface condition of the as-grown nanowires, which have never been in contact with another surface agent and have not undergone sonication or other potentially damaging dispensing procedures. Further studies are necessary to clarify these points.

With higher excitation intensity, contributions from many nanowires result in strong inhomogeneous broadening of the photoluminescence peak, as shown in Fig. 2(b). The full width at half maximum (FWHM) of the ensemble of nanowires here is 60 meV. For the time-resolved measurements, maintaining constant excitation conditions with a reasonable signal-to-noise ratio over a wide temperature range requires stronger excitation conditions compared to the time-integrated measurement. The ensemble emission intensity linearly varies over the entire excitation range investigated in either case. Although single-wire contributions are not visible with the 10 μJ/cm^2 excitation fluence used here, valuable information about the recombination dynamics is obtained by performing time-resolved photoluminescence measurements at different emission energies across the ensemble. These are depicted in Fig. 2(b), with the vertical lines indicating the energies where transient measurements were performed. This spectral dependence is repeated at various temperatures over a 4–110 K range in order to track the thermal evolution of the recombination dynamics, and the dependence on the excitation fluence is measured at 4 K.

III. RESULTS

Given the high surface-to-volume ratio of the nanowires, we might reasonably expect a monoexponential decay with a time scale determined by a fast nonradiative recombination of the sidewalls: $\tau_{\mathrm{decay}}^{-1}=\tau_{\mathrm{rad}}^{-1}+\tau_{\mathrm{nonrad}}^{-1}$, as has been seen in quantum wire structures of various materials,[21,27] which means that $\tau_{\mathrm{decay}}^{-1}\simeq\tau_{\mathrm{nonrad}}^{-1}$ when nonradiative decay dominates. However, the decay process is clearly not a simple exponential, as demonstrated in the semilogarithmic plot in Fig. 3(a) for a temperature of 20 K at various detection en-

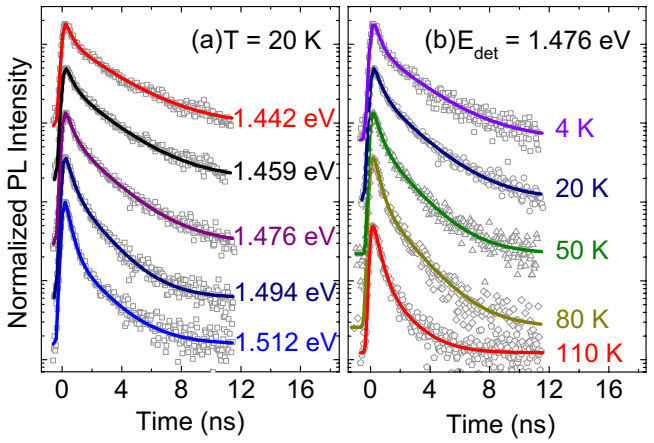

FIG. 3. (Color online) Time-resolved PL traces at (a) various detection energies for $T=20$ K and (b) various temperatures for a detection energy of 1.476 eV. Traces are vertically offset for clarity. The dots represent raw experimental data, and the solid lines are the results of the Gaussian-biexponential convolution fitting.

ergies. The basic feature of the luminescence transient is instead a distinct biexponential decay character. The fast time scale has a value of ~400 ps, and the slow time scale varies from ~2 to 5 ns depending on the emission energy and temperature, as seen in Fig. 3(b). Because this fast decay is almost comparable to the ~100 ps timing resolution of the measurement system, we extract the values of the decay times by a deconvolution procedure with the detection system. Specifically, we model the system response as a Gaussian rise time to the recorded decay curves and convolve this with two exponential decay terms of the form $A_i e^{-t/\tau_i}$. The analytic expression for this convolution is then

$$I(t) = y_0 + \sum_{i=1,2} A_i \sqrt{\frac{\pi}{2}} \left(\frac{\sigma}{\tau_i}\right) e^{\sigma^2/2\tau_i^2} e^{-(t-t_0)/\tau_i} \times \left\{1 - \mathrm{erf}\left[\frac{1}{\sqrt{2}}\left(\frac{\sigma}{\tau_i} + \frac{t_0 - t}{\sigma}\right)\right]\right\},$$

where σ is the width of the Gaussian (~100 ps), y_0 accounts for the noise floor, τ_i ($i=1,2$) are the two decay times, and A_i are the prefactors giving the relative weight of each decay process. This expression is used to fit the recorded traces over several pulse repetitions, such that the extracted values are implicitly averaged over a few cycles.

The convolution fitting procedure reproduces the observed luminescence decay extremely well, as depicted by the solid curves in Fig. 3. As is evident from these traces, the higher-energy side of the ensemble exhibits a faster effective decay time, either because of a greater contribution of the fast process or because of faster time constants. We can differentiate these factors by examining the trends associated with the extracted A_i and τ_i values individually. Figure 4 shows the variation of the decay time across the detection energies investigated over a temperature range of 4–110 K. At 4 K, the slow decay time τ_{slow} decreases from 4.7 to 2.0 ns over the 70 meV range of detection energies, while the fast decay time τ_{fast} decreases by a similar factor from 0.7 to

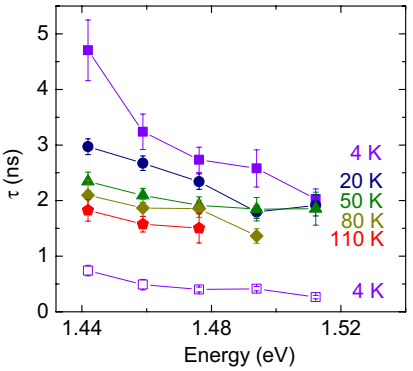

FIG. 4. (Color online) Spectral dependence of the two extracted decay times, with solid symbols for the slow time scale and open symbols for the fast time scale. τ_{fast} is not plotted for $T \geq 20$ K, since it is independent of detection energy, with a value of ~400 ps.

0.3 ns over this energy range. However, the spectral variation of the fast process is unique to the very low temperature regime. By 20 K, τ_{fast} shows no variation with the detection energy within the error of the measurement, and so is only plotted for $T=4$ K in Fig. 4. The constant value of about 400 ps for all energies suggests that thermally activated nonradiative recombination determines the time scale of this fast process for $T \geq 20$ K. This correlates with observations from an earlier study on InP nanowires synthesized under somewhat different growth conditions, which did not epitaxially grow on the substrate.[28] On the other hand, while the spectral variation of τ_{slow} weakens with increasing temperature, it is still observable at 110 K, the highest temperature investigated here.

We can gain further insight into the recombination dynamics by noting how the relative weights of the two processes change with emission energy, as shown in Fig. 5(a). Plotted is the fractional contribution of the fast process to the total decay, which is determined from the prefactors of the fitting function: $A_{fast}/(A_{fast}+A_{slow})$. For $T \leq 20$ K, the contri-

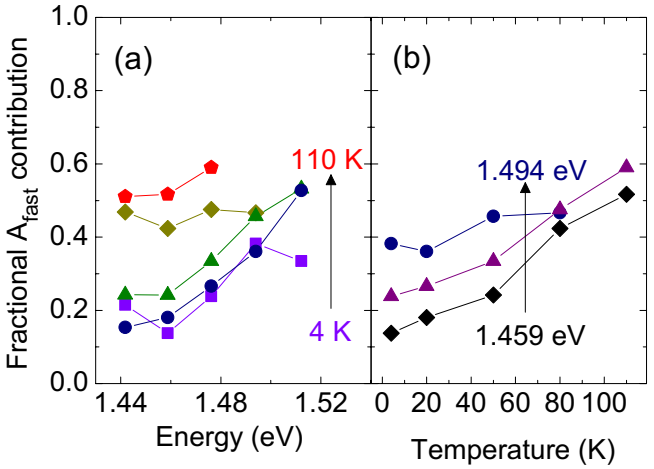

FIG. 5. (Color online) Relative weight of the fast decay process versus (a) detection energy and (b) temperature. The fast decay is more important at higher emission energies and higher temperatures.

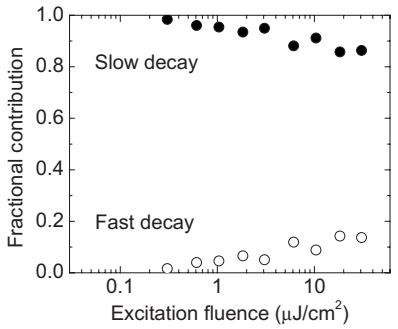

FIG. 6. Relative contribution of the slow (solid symbols) and the fast (open symbols) processes to the total decay under different excitation conditions. The decay at fluences of less than 0.3 $\mu J/cm^2$ is monoexponential with the long decay time.

bution of the fast decay increases from about 15% at a detection energy of 1.442 eV to about 50% at 1.512 eV. With increasing temperature, this fast process increasingly becomes important across the spectrum, equally contributing to the slow process even on the red side of the PL peak at 80 K. The temperature dependence of the fractional contribution of the fast decay is explicitly displayed in Fig. 5(b), with only three detection energies shown for clarity. Evidently, the fast decay process becomes increasingly significant at high emission energies and high temperatures. Nonradiative contributions to this process by 20 K in conjunction with its increasing relative weight with temperature imply that the fast decay plays a critical role in quenching of the PL intensity at elevated temperatures.

The spectral and thermal dependences of the biexponential decay characteristics are performed under constant excitation conditions, at a fluence of 10 $\mu J/cm^2$, in order to avoid complicating the results with a third variable. We separately examine the role of the excitation conditions by measuring the PL decay at the peak energy of the ensemble at 4 K by varying excitation fluence over 2 orders of magnitude. Here, the key finding is that under very low excitation conditions, the luminescence decay is monoexponential rather than biexponential, with the time scale given by the slow decay time. At a fluence of 0.3 $\mu J/cm^2$, the biexponential character begins to appear. The absolute decay time values vary little with excitation over the 0.06–12 $\mu J/cm^2$ range investigated. The slow decay time slightly decreases from 3.8 to 3.2 ns over this range, while the fast decay time remains constant at 0.7 ns. The transition from a monoexponential to biexponential decay character is demonstrated in Fig. 6 by comparing the relative weights of the slow and fast processes. The fractional contribution of the fast process increases from 0 below 0.3 $\mu J/cm^2$ to about 15% at the highest fluence level of 12 $\mu J/cm^2$.

IV. DISCUSSION

The origin of the two exponential decay terms in the time-resolved traces in InP nanowires has previously been ascribed to band bending due to a large density of surface states on the nanowires.[3] This argument was originally formulated to describe the strong blueshift seen with increasing

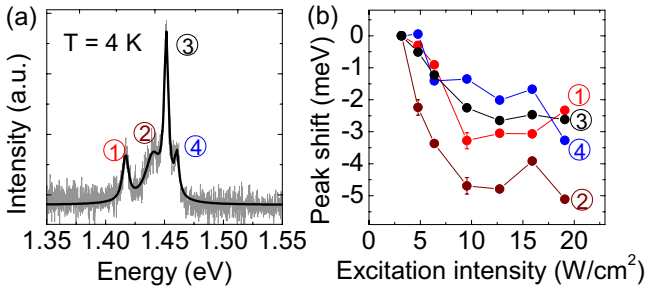

FIG. 7. (Color online) (a) Spectrum showing four narrow emission lines (FWHM ~4–6 meV) taken with an excitation intensity of 4.8 W/cm^2. The thick solid line is the sum of the four Lorentzian functions used to fit the spectrum. (b) Change in the peak position (1–4) as a function of excitation intensity from the lowest excitation used, 3.2 W/cm^2. All peaks redshift with increasing excitation.

excitation intensity of the time-integrated PL peak of *p*-doped InP nanowires.[7] With few photo- (or thermally) excited charge carriers, band bending effectively localizes one carrier type at the surface and the other carrier type in the center of the wire, resulting in spatially indirect recombination at a lower energy than the flat-band condition. With a large number of photoexcited carriers, such as with strong cw excitation or immediately after an excitation pulse, the bands are flattened and recombination occurs at a comparatively higher energy. In this picture, a signature of the band-bending phenomenon is a blueshift of the PL peak with increasing excitation intensity. However, it is crucial to differentiate between the behavior of the ensemble and the behavior of individual nanowire peaks under increasing excitation. Here, we do see a blueshift of the *ensemble* peak of about 17 meV from low excitation conditions to the 10 $\mu J/cm^2$ used in the measurements described above, much smaller than the 70 meV/decade shift observed in *p*-doped InP wires.[7] The narrow, single-wire peaks as in Fig. 2(a), in fact, show a slight *redshift* with increasing intensity even under low excitation conditions, as would be expected for band gap renormalization[23] or from simple beam-induced heating.

We can examine this in greater detail by tracking the peak energy of single-wire luminescence peaks under varying cw excitation ($\lambda = 532$ nm). Figure 7(a) shows four such peaks measured with an excitation intensity of 4.8 W/cm^2, with the primary peak having a FWHM of 4.3 meV. The four features can be fit extremely well by a sum of four Lorentzians, which are indicated by the thick solid line in Fig. 7(a). Repeating this fitting for spectra taken under different excitation intensities, the peak energy can be compared to its position measured under the lowest excitation conditions, $I = 3.2$ W/cm^2. This shift is plotted for each peak in Fig. 7(b), revealing a small but consistent decrease in peak energy with increasing excitation intensity. The size of this redshift ranges from ~3 to 5 meV over the range of intensities used here, which likely only measurable because of the narrow linewidths involved. The cw range of excitation densities corresponds to purely monoexponential decay in the time-resolved measurements.

These measurements clearly demonstrate that the shift of the ensemble does not reflect the behavior of individual

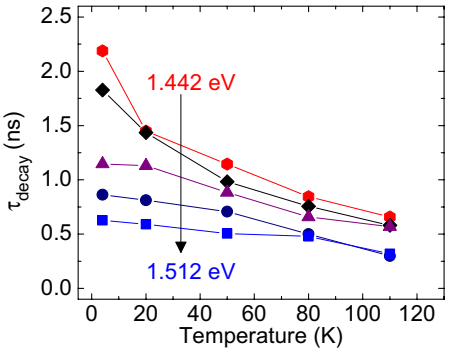

FIG. 8. (Color online) The effective decay time is larger for redder emission energies than bluer ones, but consistently decreases with temperature.

nanowires under increasing excitation. We believe that the explanation for this apparent contradiction is quite simple: band filling, rather than band bending. That is, the ensemble exhibits a blueshift with increasing excitation because higher subbands of the nanowires are directly observable in the luminescence spectrum under strong photoexcitation. The slight redshift associated with individual nanowire peaks is masked by the increasing contribution of luminescence from $n>1$ energy levels of the many nanowires involved in the overall ensemble signal. Thus, while we associate the ensemble blueshift with band filling, we must disassociate the origin of the biexponential PL decay from earlier band-bending arguments for the nanowires investigated in this study.

On the other hand, biexponential PL decay characteristics have been observed in quantum wire structures of both III-V and II-VI materials to the describe dynamics[24,25,29] of excitons, which may account for the narrow luminescence peaks observed. The exciton binding energy, which strongly depends on the structure size and confinement potential, is well known to be enhanced from the bulk value in quantum wells and has been shown to have an even larger enhancement in quantum wires with lateral dimensions of less than 50 nm.[30] This binding energy should be exceptionally large compared to bulk InP[16] for the nanowires investigated here, given that the diameters are small and the surrounding material is air. In the exciton picture, the fast and slow processes of the biexponential decay can be associated with free and localized excitons, respectively, and the relative weight of each decay process depends on the ratio of the number excitons generated in a laser pulse to the number localization centers present in the wire.[25] The monoexponential behavior under low excitation ($\leq 0.3\ \mu J/cm^2$) then corresponds to the localized exciton lifetime. We can define an effective decay time, plotted in Fig. 8, by writing $\tau_{decay}^{-1}=A_{fast}\tau_{fast}^{-1}+A_{slow}\tau_{slow}^{-1}$, which is equivalent to the expression $\tau^{-1}=N_{total}^{-1}(N_{free}\tau_{free}^{-1}+N_{loc}\tau_{loc}^{-1})$, which is used to describe populations of free and localized excitons, where the total exciton density, $N_{total}=N_{free}+N_{loc}$, is the sum of the component free and localized exciton densities.[31] This effective decay time, which implicitly includes nonradiative contributions through the A_i and τ_i values, is plotted in Fig. 8. For a coarse estimate of the localization energy, we can make a simple Arrhenius plot of the integrated intensity of the ensemble, which yields a value of 7.8 meV. Since this energy comes from the intensity change of the whole distribution of nanowires, it should be regarded as the average for all of the different wire sizes. We note, however, that this localization energy is larger than the collection bandwidth in the measurement, implying that for a given detection energy, the slow and fast decay components arise from distinct nanowires. Future measurements investigating single nanowires should result in a clearer picture of the relationship between the exciton localization energy and emission energy or wire size.

V. CONCLUSION

In summary, we have performed a systematic study of the recombination dynamics of the as-grown wurtzite InP nanowires depending on emission energy, temperature, and excitation fluence. Time-integrated PL measurements reveal linewidths of a few meV, and corresponding transient measurements point to a biexponential decay process, with a fast time scale of 0.3–0.7 ns and a slow time scale ranging from 2 to 4.7 ns at $T=4$ K. The fractional contribution of each process to the total decay is determined from the deconvolution fitting procedure, indicating a comparatively small contribution of the fast decay at low (redder) emission energies at low temperatures and a vanishing contribution under low excitation conditions. The slight redshift associated with individual narrow luminescence peaks under increasing excitation intensity is inconsistent with the band-bending phenomenon described in other InP nanowire studies, implying that the two-component decay has a different origin. We propose that this may be due to exciton localization effects, observed in a variety of III-V and II-VI quantum wire structures and freestanding II-VI nanorods but not reported in freestanding III-V nanowires. The decay times observed in these as-grown nanowires may serve as a basis of comparison for surface-treated nanowires, including both passivation treatments and unintentional surface modification by fabrication processing steps of nanowire-based devices.

ACKNOWLEDGMENTS

The authors acknowledge project support from DARPA (Grant No. HR0011-04-1-0040 CONSRT) and HP-CITRIS grants, as well as the IST Project Node of the European Commission and the State of Bavaria. Author support is acknowledged from the NSF-GRFP (S.C.), and NSF-IGERT (L.C.C., M.M., S.C.) programs.

[1] X. Duan and C. Lieber, Adv. Mater. (Weinheim, Ger.) **12**, 298 (2000).
[2] M. W. Larsson, J. B. Wagner, M. Wallin, P. Hakansson, L. E. Froberg, L. Samuelson, and L. R. Wallenberg, Nanotechnology **18**, 015504 (2007).
[3] M. Mattila, T. Hakkarainen, H. Lipsanen, H. Jiang, and E. I. Kauppinen, Appl. Phys. Lett. **90**, 033101 (2007).
[4] P. Mohan, J. Motohisa, and T. Fukui, Nanotechnology **16**, 2903 (2005).
[5] P. Mohan, J. Motohisa, and T. Fukui, Appl. Phys. Lett. **88**, 013110 (2006).
[6] R. S. Wagner and W. C. Ellis, Appl. Phys. Lett. **4**, 89 (1964).
[7] M. H. M. van Weert, O. Wunnicke, A. L. Roest, T. J. Eijkemans, A. Yu Silov, J. E. M. Haverkort, G. W. 't Hooft, and E. P. A. M. Bakkers, Appl. Phys. Lett. **88**, 043109 (2006).
[8] S. Bhunia, T. Kawamura, S. Fujikawa, H. Nakashima, K. Furukawa, K. Torimitsu, and Y. Watanabe, Thin Solid Films **464-465**, 244 (2004).
[9] L. C. Chuang, M. Moewe, C. Chase, N. Kobayashi, C. Chang-Hasnain, and S. Crankshaw, Appl. Phys. Lett. **90**, 043115 (2007).
[10] S. J. May, J.-G. Zheng, B. W. Wessels, and L. J. Lauhon, Adv. Mater. (Weinheim, Ger.) **17**, 598 (2005).
[11] M. Mattila, T. Hakkarainen, M. Mulot, and H. Lipsanen, Nanotechnology **17**, 1580 (2006).
[12] L. C. Chuang, M. Moewe, S. Crankshaw, and C. Chang-Hasnain, Appl. Phys. Lett. **92**, 013121 (2008).
[13] M. S. Gudiksen, J. Wang, and C. M. Lieber, J. Phys. Chem. B **106**, 4036 (2002).
[14] J. Tragardh, A. I. Persson, J. B. Wagner, D. Hessman, and L. Samuelson, J. Appl. Phys. **101**, 123701 (2007).
[15] M. Murayama and T. Nakayama, Phys. Rev. B **49**, 4710 (1994).
[16] T. Akiyama, K. Nakamura, and T. Ito, Phys. Rev. B **73**, 235308 (2006).
[17] H. Akiyama, S. Koshiba, T. Someya, K. Wada, H. Noge, Y. Nakamura, T. Inoshita, A. Shimizu, and H. Sakaki, Phys. Rev. Lett. **72**, 924 (1994).
[18] N. I. Cade, R. Roshan, M. Hauert, A. C. Maciel, J. F. Ryan, A. Schwarz, Th. Schäpers, and H. Lüth, Phys. Rev. B **70**, 195308 (2004).
[19] D. Y. Oberli, M.-A. Dupertuis, F. Reinhardt, and E. Kapon, Phys. Rev. B **59**, 2910 (1999).
[20] M. Lomascolo, P. Ciccarese, R. Cingolani, R. Rinaldi, and F. K. Reinhart, J. Appl. Phys. **83**, 302 (1998).
[21] F. Kieseling, W. Braun, P. Ils, M. Michel, A. Forchel, I. Gyuro, M. Klenk, and E. Zielinski, Phys. Rev. B **51**, 13809 (1995).
[22] D. Fuster, J. Martinez-Pastor, L. Gonzalez, and Y. Gonzalez, Phys. Rev. B **71**, 205329 (2005).
[23] L. Titova, T. B. Hoang, J. M. Yarrison-Rice, H. E. Jackson, Y. Kim, H. J. Joyce, Q. Gao, H. H. Tan, C. Jagadish, X. Zhang, J. Zou, and L. M. Smith, Nano Lett. **7**, 3383 (2007).
[24] L. Wischmeier, T. Voss, I. Rückmann, J. Gutowski, A. C. Mofor, A. Bakin, and A. Waag, Phys. Rev. B **74**, 195333 (2006).
[25] K. Herz, G. Bacher, A. Forchel, H. Straub, G. Brunthaler, W. Faschinger, G. Bauer, and C. Vieu, Phys. Rev. B **59**, 2888 (1999).
[26] L. V. Titova, T. B. Hoang, H. E. Jackson, L. M. Smith, J. M. Yarrison-Rice, J. L. Lensch, and L. J. Lauhon, Appl. Phys. Lett. **89**, 053119 (2006).
[27] R. Spiegel, G. Bacher, K. Herz, M. Illing, T. Kümmell, A. Forchel, B. Jobst, D. Hommel, G. Landwehr, J. Söllner, and M. Heuken, Phys. Rev. B **53**, R4233 (1996).
[28] S. Reitzenstein, S. Münch, C. Hofmann, A. Forchel, S. Crankshaw, L. C. Chuang, M. Moewe, and C. Chang-Hasnain, Appl. Phys. Lett. **91**, 091103 (2007).
[29] D. Fuster, J. Martínez-Pastor, L. González, and Y. González, J. Phys. D **39**, 4940 (2006).
[30] M. Bayer, S. N. Walck, T. L. Reinecke, and A. Forchel, Phys. Rev. B **57**, 6584 (1998).
[31] D. S. Citrin, Phys. Rev. B **47**, 3832 (1993).